Experimental Mechanics (2021) 61:1237–1247
https://doi.org/10.1007/s11340-021-00726-5

RESEARCH PAPER

DLT-Lines Based Camera Calibration with Lens Radial and Tangential Distortion

Z. C. Shi[1,2] · Y. Shang[1,2] · X. F. Zhang[3] · G. Wang[1,2]

Received: 5 October 2020 / Accepted: 20 April 2021 / Published online: 22 June 2021

Abstract

Background Camera calibration is an essential step for the optical measurement method used in the experimental mechanics. Most plumb line methods focus on solving lens distortions without considering camera intrinsic and extrinsic parameters.

Objective In this paper, we propose a full camera calibration method to estimate the camera parameters, including camera intrinsic parameters, extrinsic parameters and lens distortion parameters, from a single image with six or more non-coplanar lines.

Methods We parameterize the 3D lines with the intersection of two planes that allow the direct linear transformation of the lines(DLT-Lines). Based on the DLT-Lines, the projection matrix is estimated linearly, and then the camera intrinsic and extrinsic parameters are extracted from the matrix. The relationship between the distorted 2D lines and the distortion coefficients is derived, based on which the distortion coefficients can be solved linearly. In the last step, a non-linear optimization algorithm is used to jointly refine all the camera parameters, including the distortion coefficients.

Results Both synthetic and real data are used to evaluate the performance of our method, which demonstrates that the proposed method can calibrate the cameras with radial and tangential distortions accurately.

Conclusions We propose a DLT-lines based camera calibration method for experimental mechanics. The proposed method can calibrate all the camera parameters from a single image.

Keywords DLT-Lines · Camera calibration · Lens distortion · Plumb line method

Introduction

Optical measurement, such as digital image correlation (DIC), is a basic technique in experimental mechanics. It is widely used in many practical tasks, such as target 3D shape, deformation measurements [1, 2], and motion parameters measurements [3, 4]. The accurate calibration parameters of the camera are essential to the optical measurement deployed for applications in the experimental mechanics [5–7].

Camera calibration is the task of determining the camera imaging model and the lens distortion model. It is an important and fundamental step in many computer vision and photogrammetry applications, such as 3D reconstruction, augmented reality, robotic navigation, and so on. The pin-hole imaging model is most widely used, which contains the camera's intrinsic and extrinsic parameters. Ideally, it maps straight lines in the 3D projective space to the 2D image lines, which are also straight. Considering the lens distortion, which is widely existed in the optical system, the ideal imaging is no longer available. Thus, the pin-hole model and the distortion model needed to be estimated accurately and simultaneously.

Generally, camera calibration methods can be categorized into known pattern calibration methods [8–10] and self-calibration methods [11–15]. The later usually calibrate the intrinsic parameters only by utilizing the non-metric information, such as the image of the absolute quadratic curve [14]. The former utilizing the 3D or 2D known pattern to learn the correspondences between the features of

Z. C. Shi and Y. Shang both are equally contributed.

✉ Y. Shang
shangyang1977@nudt.edu.cn

[1] College of Aerospace Science and Engineering, National University of Defense Technology, Changsha 410073, China

[2] Hunan Provincial Key Laboratory of Image Measurement and Vision Navigation, Changsha 410073, China

[3] Jiuquan Satellite Launch Center, Jiuquan 732750, China

the real-world and their counterparts lying in the image plane. It computes the intrinsic, extrinsic parameters and distortion model simultaneously, hence it is the full camera calibration method. Tsai [9] proposed the two-step calibration technique with the 3D non-coplanar points. Zhang [10] presented a flexible technique for camera calibration utilizing a 2D pattern, which is captured from different viewpoints by the camera.

The distortion model can be calibrated alone [16–20] or together [21] with the camera intrinsic and extrinsic parameters. Intuitively, the lines are born to be suitable for calibrating the lens distortion as the facts that straight lines have to be straight, and approaches based on this projective invariant are known as plumb line methods [19]. Based on this observation, Devernay et al. [19] proposed the method that fitting the 2D lines iteratively to compute the distortion parameters. Melegy et al. [22] utilized the the-least-median-of-squares estimator to discard the outliers in the data for fitting the corrected image lines. Then the distortion parameters are computed from the straightened lines. Benligiray et al. [17] calculated the radial distortion by utilizing the groups of lines. These plumb line methods are practical for straightening the image lines. Besides, they are feasible to the case that the camera is unavailable for the calibration process. However, plumb line methods neglect the fact that the distortion parameters are most often coupled with internal camera parameters. This may results in that we may obtain the straightened parameters but not the actual distortion parameters.

Here, we present a full calibration method for camera calibration from a single image with six or more non-coplanar 3D lines. The proposed method is related to the methods based on the correspondences between the 3D control points and their image projections, named Direct Linear Transformation (DLT) [23]. This type of method solves the camera pose, camera intrinsic parameters, and camera lens distortion parameters jointly. More recently, recent works [21, 24, 25] have shown that line correspondences are less sensitive to noise, which can reduce the match error between the 3D points and 2D image points. Besides, the line correspondence could be used to calibrate the camera parameters just like the point correspondence. Hence, we aim at conducting the calibration task with the 3D lines instead of 3D points. The proposed method is also based on the fact that the imaged lines of 3D lines in the 3D projective space need to be straight. Moreover, the proposed method couples the distortion parameters with the camera intrinsic parameters by involving the 2D reprojection lines for estimating the distortion model. More specifically, we first estimate the camera intrinsic and extrinsic parameters by utilizing the direct linear transformation (DLT) of lines. Then the projection of the lines is calculated and used to compute the distortion parameters, followed by a non-linear optimization process. With the proposed method, the distorted lines are not only straightened but also their corresponding points that lie on the lines are corrected with camera intrinsic parameters and distortion parameters. Our contributions can be summarized as follow:

- We present a full calibration method for camera calibration, which estimates the camera intrinsic, extrinsic parameters, and lens distortion parameters, simultaneously. The solutions of all calibration parameters are received linearly and analytically.
- We parameterize 3D lines with two planes that allow linear projections of the 3D lines. Consequently, the distortion parameters are coupled with the camera's intrinsic parameters as they are calculated with the reprojection lines. Both lens radial and tangential distortion parameters are calculated.
- The synthetic data and real scene data experiments validate that the proposed method is practical for vision based measurement applications.

The remainder of this paper is organized as follows. Section 2 introduces the pin-hole imaging model and the camera lens distortion model that contains the radial and tangential distortion. In Section 3, the DLT-Lines based calibration method is described. Section 4 presents the synthetic data and real scene data experiments to validate the proposed method. Section 5 draws the conclusions.

Preliminaries

Ideal Imaging Model

The pin-hole imaging model maps the 3D projective space to the 2D image plane by perspective projection, see Fig. 1. A 3D point is represented in homogeneous coordinates as

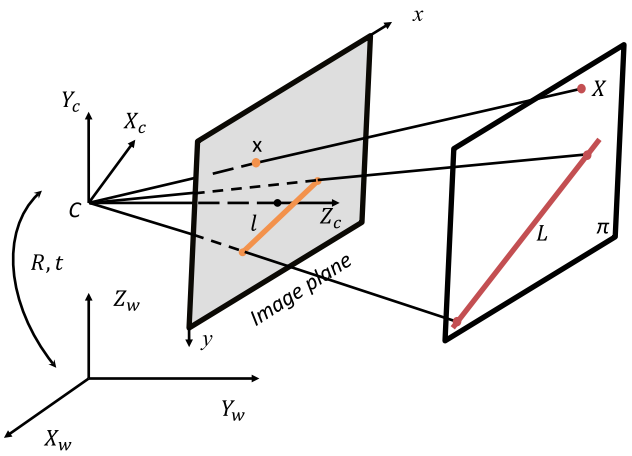

Fig. 1 The pin-hole imaging model of point and line

a 4-vector, $\mathbf{X} = [x\ y\ z\ w]^T$, with $w = 0$ represents the point at infinity. Generally, a regular point $[x\ y\ z]^T$ of $\mathbb{R}^3$ is represented as $\mathbf{X} = [x\ y\ z\ 1]^T$ with $w = 1$. Similarly, a homogeneous representation of a 2D point is $\mathbf{x} = [x\ y\ 1]^T$. With the homogeneous representation, the pin-hole imaging model maps the 3D point into the 2D image plane as follow:

$$\lambda \mathbf{x} = \mathbf{M}\mathbf{X} = \mathbf{K}[\mathbf{R} \quad \mathbf{t}]\mathbf{X} \tag{1}$$

where λ is a depth scale factor, $\mathbf{X}$ and $\mathbf{x}$ are homogeneous coordinates of a 3D point and its corresponding 2D image planar point, respectively. The rotation matrix $\mathbf{R}$ and translation vector $\mathbf{t} = [t_x\ t_y\ t_z]^T$ are named as extrinsic parameters and form the rigid transformation from the world coordinate frame to the camera coordinate frame. More specifically, $\mathbf{t}$ denotes the coordinates of the origin of the world frame in the camera frame and $\mathbf{R}$ represents three axes unit vectors of the world frame in the camera frame. $\mathbf{K}$ is an upper triangular matrix, named camera intrinsic matrix, as shown in equation (2), it contains the effective focal lengths of two coordinate axes (f_x,f_y), and the location of principal point (c_x, c_y). Note that we assume the skew factor is zero and the intrinsic matrix only contains the aforementioned 4 parameters.

$$\mathbf{K} = \begin{bmatrix} f_x & 0 & c_x \\ 0 & f_y & c_y \\ 0 & 0 & 1 \end{bmatrix} \tag{2}$$

Camera Lens Distortion Model

The ideal pin-hole imaging model describes the relationship between the 3D point and its corresponding image point. However, lens distortion induces a non-constant offset δ between the actual image point x_d and the ideal image point x_u given by the pin-hole imaging model. For high accuracy calibration, the lens distortion needs to be considered and modeled.

To model the lens distortion, we use the distortion model proposed by Weng et al. [26], which combines the radial and tangential distortion as the follow:

$$\begin{cases} \delta_x = x - x_d = f_x(k_0 r^2 u + k_1 r^2 + k_3 u^2 + k_4 uv) \\ \delta_y = y - y_d = f_y(k_0 r^2 v + k_2 r^2 + k_3 uv + k_4 v^2) \end{cases} \tag{3}$$

$$u = (x - c_x)/f_x, v = (y - c_y)/f_y \tag{4}$$

where u and v are the unobservable distortion free image coordinates, as shown in equation (4), $r^2 = u^2 + v^2$, k_0 is the coefficient of radial distortion, while k_1, k_2, k_3 and k_4 are the coefficients of tangential distortion.

Methodology

Line Representation

A line $\mathbf{l}$ in the 2D space can be defined by the join of two points $\mathbf{x}^1$, $\mathbf{x}^2$, and it can be written concisely as

$$\mathbf{l} = [a \quad b \quad c]^T = \mathbf{x}^1 \times \mathbf{x}^2 \tag{5}$$

where $\mathbf{x}^1$ and $\mathbf{x}^2$ are the homogeneous representation. A 2D point $\mathbf{x}$ lying on the line l satisfies that their inner product is zero.

$$\mathbf{x}^T\mathbf{l} = ax + by + c = 0 \tag{6}$$

Similarly, a line in 3D space is represented by the join of two points or the intersection of two planes. Without loss of generality, we use the intersection of two planes to define a 3D line, as described by equation (7), since the points and planes are dual in 3D space.

$$\begin{cases} A_1 x + B_1 y + C_1 z + D_1 = 0 \\ A_2 x + B_2 y + C_2 z + D_2 = 0 \end{cases} \tag{7}$$

where each equation denotes one plane. Homogenizing equation (7) by using the homogeneous coordinates gives concise expression

$$\mathbf{L}\mathbf{X} = \begin{bmatrix} \mathbf{P}^T \\ \mathbf{Q}^T \end{bmatrix} \mathbf{X} = \begin{bmatrix} 0 \\ 0 \end{bmatrix} \tag{8}$$

where $\mathbf{P} = [A_1 \quad B_1 \quad C_1 \quad D_1]^T$ denotes the first plane, $\mathbf{Q} = [A_2 \quad B_2 \quad C_2 \quad D_2]^T$ denotes the second plane, $\mathbf{L} = [\mathbf{P} \quad \mathbf{Q}]^T$ denotes the 3D line defined by planes $\mathbf{P}$ and $\mathbf{Q}$, and $\mathbf{X}$ is a 3D point lying on the line $\mathbf{L}$.

The 3D line could be obtained by the total station or 3D pattern because it could be represented by a collection of points. In the following, we describe how to acquire the planar representation of a 3D line using a collection of points. Once the collection of points are in the world coordinate system, the representation of 3D line is also in the world coordinate system.

We set $\{\mathbf{X}^i\}$ as a collection of points lie on a 3D line. Firstly, the centroid of $\{\mathbf{X}^i\}$ is denoted as $\mathbf{X}_c$ and the normalized direction vector $\mathbf{v}_\mathbf{L}$ of the 3D line is fitted by using $\{\mathbf{X}^i\}$. Afterward, the normal vector $\mathbf{v}_\mathbf{P} = \mathbf{v}_\mathbf{L} \times \mathbf{v}_r$ of first plane $\mathbf{P}$ is calculated, where $\mathbf{v}_r$ denotes the normalized vector of $\mathbf{v}_\mathbf{L} + [0 \quad 0 \quad 0.5]^T$. Then the first plane is obtained, $[A_1 \quad B_1 \quad C_1]^T = \mathbf{v}_\mathbf{P}$, $D_1 = -\mathbf{X}_c^T\mathbf{v}_\mathbf{P}$. Similarly, the normal vector $\mathbf{v}_\mathbf{Q} = \mathbf{v}_\mathbf{L} \times \mathbf{v}_\mathbf{P}$ of second plane $\mathbf{Q}$ is calculated and $[A_2 \quad B_2 \quad C_2]^T = \mathbf{v}_\mathbf{Q}$, $D_2 = -\mathbf{X}_c^T\mathbf{v}_\mathbf{Q}$. Finally, we obtained the 3D line represented by two planes, it could be used in the fellowing section.

DLT-Lines

The DLT applies the imaging points' vectors linear cross product to induce a linear system of the camera projection matrix. More specifically, applying a cross product by $\mathbf{x}$ to both sides of equation (1) gives

$$[\mathbf{x}]_\times \mathbf{x} = [\mathbf{x}]_\times \mathbf{M}\mathbf{X} = 0 \tag{9}$$

where $[\cdot]_\times$ is a skew-symmetric matrix of a 3D vector. $\mathbf{M}$ is the projection matrix that formed by the camera matrix $\mathbf{K}$, rotation matrix $\mathbf{R}$ and translation vector $\mathbf{t}$.

$$\mathbf{M} = \mathbf{K}[\mathbf{R} \quad \mathbf{t}] = \begin{bmatrix} m_0 & m_1 & m_2 & m_3 \\ m_4 & m_5 & m_6 & m_7 \\ m_8 & m_9 & m_{10} & m_{11} \end{bmatrix} \tag{10}$$

Flattens the projection matrix $\mathbf{M}$, which is arranged in column major, into a 12-vector $\mathbf{m}$ and utilize the Kronecker product $\otimes$ [27] gives

$$(\mathbf{X}^T \otimes [\mathbf{x}]_\times)\mathbf{m} = \mathbf{0}_{3\times 1} \tag{11}$$

Note that only two linear equations in equation (11) are linearly independent since the third one can be induced from the first two. One 3D point $\mathbf{X}$ and its corresponding 2D image point $\mathbf{x}$ induce two independent equations. By stacking a set of 3D-2D correspondences together (more than six and the 3D points are non-coplanar), the entries of projection matrix $\mathbf{M}$ are estimated by solving the linear system.

As shown in Fig. 1, the pure pin-hole imaging model maps a 3D line to a 2D line without considering the lens distortion. Note that once the 3D line through the optical center, its image is not a line but a single point, which is a degeneration case.

Without loss of generality, assuming the 3D line expressed in equation (7) is not perpendicular to the axis x, it can be rewritten as

$$\begin{cases} x = \frac{-(A_1C_2 - A_2C_1)x + (C_1D_2 - C_2D_1)}{B_1C_2 - B_2C_1} = \frac{-\iota_1 x + \iota_3}{\iota_0} \\ z = \frac{(A_1B_2 - A_2B_1)x - (B_1D_2 - B_2D_1)}{B_1C_2 - B_2C_1} = \frac{\iota_2 x - \iota_4}{\iota_0} \end{cases} \tag{12}$$

Note that the aforementioned assuming condition is just for deriving conveniently, but not a requirement for calibration.

According to equation (6), a 2D image point $\mathbf{x}$ lies on $\mathbf{l}$ if and only if their inner product is zero. Consequently, analogous to the DLT-points shown in equation (11), we apply the inner product by $\mathbf{l}$ to both sides of equation (1) and we can obtain the following equation,

$$\mathbf{l}^T\mathbf{x} = \mathbf{l}^T\mathbf{M}\mathbf{X} = 0 \tag{13}$$

where $\mathbf{l}$ is the projection of the 3D line $\mathbf{L}$, $\mathbf{X}$ is a 3D projective space point lies on $\mathbf{L}$. It maps all the 3D points that lie on a line to one 2D line, which means the correspondences are many 3D-points to one 2D-line $(\mathbf{l}, \mathbf{X}^i)$.

Applying equation (12) to equation (13), we can derive one linear equation that contains the projection matrix $\mathbf{M}$ and 3D line parameters $\mathbf{L}$,

$$\phi(\mathbf{M}, \mathbf{L})x + \varphi(\mathbf{M}, \mathbf{L}) = 0 \tag{14}$$

where x is the coordinate value of the 3D point $\mathbf{X}$; ϕ and φ represent the coefficients derived from the projection matrix $\mathbf{M}$ and 3D line $\mathbf{L}$. From (14), we know that all points lie on the 3D line mapped into one 2D line. In other words, for X of any 3D point lies on line satisfies equation (14). Consequently, we could conclude that $\phi(\mathbf{M}, \mathbf{L})$ and $\varphi(\mathbf{M}, \mathbf{L})$ must be 0 and form two linear equations for one line.

$$\begin{cases} \phi = a(m_0\iota_0 - m_1\iota_1 + m_2\iota_2) + \\ \qquad b((m_4\iota_0 - m_5\iota_1 + m_6\iota_2)) + \\ \qquad c(m_8\iota_0 - m_9\iota_1 + m_{10}\iota_2) = 0 \\ \varphi = a(m_1\iota_3 - m_2\iota_4 + m_3\iota_0) + \\ \qquad b(m_5\iota_3 - m_6\iota_4 + m_7\iota_0) + \\ \qquad c(m_9\iota_3 - m_{10}\iota_4 + m_{11}\iota_0) = 0 \end{cases} \tag{15}$$

where $\iota_i, (i = 0, 1, 2, 3, 4)$ are defined in equation (12), $m_i, (i = 0, 1, \cdots, 11)$ are the entries of projection matrix.

Since a 2D line is specified by two independent parameter ratios $\{a : b : c\}$, it can be solved from equation (15). Hence, equation (15) maps a 3D line to a 2D line and forms the one 3D-line to one 2D-line correspondence $(\mathbf{L}_j, \mathbf{l}_j)$.

To estimate the projection matrix, by considering the fact that $m_{11} = t_z > 0$, which means the object must be in front of the camera if it can be captured by the camera, we denote $\mathbf{S}$ as

$$\mathbf{S} = \frac{1}{m_{11}}\mathbf{M} = \begin{bmatrix} s_0 & s_1 & s_2 & s_3 \\ s_4 & s_5 & s_6 & s_7 \\ s_8 & s_9 & s_{10} & 1 \end{bmatrix} = \begin{bmatrix} \mathbf{s}_0 & \mathbf{s}_1 & \mathbf{s}_2 & \mathbf{s}_3 \end{bmatrix} \tag{16}$$

where the j-th column of matrix $\mathbf{S}$ is denoted by $\mathbf{s}_j$. Then the equation (15) could be rearranged as follow:

$$\begin{bmatrix} \iota_0\mathbf{l}^T & -\iota_1\mathbf{l}^T & \iota_2\mathbf{l}^T & \mathbf{0} \\ \mathbf{0} & \iota_3\mathbf{l}^T & -\iota_4\mathbf{l}^T & \iota_0\mathbf{l}^T \end{bmatrix} \begin{bmatrix} \mathbf{s}_0 \\ \mathbf{s}_1 \\ \mathbf{s}_2 \\ \mathbf{s}_3 \end{bmatrix} = \mathbf{H}_j\mathbf{s} = \begin{bmatrix} 0 \\ 0 \end{bmatrix} \tag{17}$$

Each pair of 3D line and its corresponding image line $(\mathbf{L}_j, \mathbf{l}_j)$ provides two linear constraints in the vectorization of projection matrix $\mathbf{S}$. Once given $N \geqslant 6$ pairs $(\mathbf{L}_j, \mathbf{l}_j)$, one form two linear equations, a linear system ($2N$ equations) could be build by stacking the set of equations derived from equation (17). Note that $[m_8\ m_9\ m_{10}]$ is the third-row vector of rotation matrix and its norm is 1, once the $\mathbf{s}$ is calculated, m_{11} could be calculated by $m_{11} = 1/\left\|[s_8\ s_9\ s_{10}]\right\|$. Consequently, the projection matrix could be estimated by solving the linear system.

Once the projection matrix is estimated, as shown in equation (10), camera intrinsic matrix **K** and the rotation matrix **R** could be calculated by using the QR-decomposition. The translation vector **t** could be extracted from the projection matrix directly.

Solving for Lens Distortion Coefficients

In the lens distortion model, the distorted offset is calculated by the ideal image point. However, the ideal image point could not be obtained before the distortion coefficients is estimated. In this paper, we use the distorted image point to compute the distorted offset iteratively with the facts that the distorted image point is close to ideal image point by being corrected iteratively.

As shown in equation (3), the lens with radial and tangential distortion is modeled by the corresponding coefficients. Apply equation (3) and (4) to equation (6) gives

$$\begin{aligned}&(af_x u + bf_y v)r^2 k_0 + af_x r^2 k_1 + \\ &bf_y r^2 k_2 + (af_x u^2 + bf_y uv)k_3 + \\ &(af_x uv + bf_y u^2)k_4 = ax_d + bx_d + c\end{aligned} \tag{18}$$

Given a projective 2D line $\mathbf{l} = [a \quad b \quad c]^T$ and its a corresponding set of distorted points $\{\mathbf{x}_d^i\}$ in the image plane, we could compute the lens distortion coefficients from the over-determined linear system equations.

Calibration with Distortion

The calibration based on the DLT-lines is summarized in algorithm 1, see Algorithm 1. The input to the algorithm are $N \geqslant 6$ non-coplanar 3D lines and their corresponding image lines in a single image; and the output are the estimated camera intrinsic matrix, distortion coefficients, and the extrinsic parameters that contain rotation matrix and translation vector. The camera projection matrix **M** is firstly obtained by solving a linear system equations and then is used to project the 3D lines. Afterward, the distortion coefficients are calculated by using the reprojection lines and their corresponding distorted image points. The image points that lying on the image lines are corrected using the distortion model from equation (3).

After the linear solution of the camera projection matrix and the distortion parameters are obtained, we utilize the Levenberg-Marquardt algorithm to jointly refine the camera matrix and the distortion coefficients by minimizing the image points to image line distance, as the follow:

$$F(\mathbf{M}, \mathbf{k}) = arg \min_{\mathbf{M},\mathbf{k}} \sum_j^N \sum_i \frac{(a_j x_d^{ji} + b_j y_d^{ji} + c_j)^2}{a_j^2 + b_j^2} \tag{19}$$

where the $[a_j \quad b_j \quad c_j]$ represent the j–th reprojection line using the projection matrix **M** and the distortion model from equation (3); (x_d^{ji}, y_d^{ji}) denotes the distorted point that lies on the corresponding image line. The proposed method technically requires at least 6 non-coplanar 3D lines and their corresponding projection lines to calibrate all the camera parameters, including the intrinsic, extrinsic parameters, and distortion parameters. It does not require additional lines to calibrate the distortion parameters. It also should be noted that though large N is not necessary, 10 to 15 is recommended and the selected projection lines should extend over the image region to get a good calibration result.

Algorithm 1 DLT-lines based Levenberg–Marquardt algorithm strategy calibration

Input:

$\{\mathbf{L}_j\}-$ 3D lines, $\{\mathbf{l}_j\}-$ 2D image lines, T, $t = 0$.

Output:

$\mathbf{K}-$ camera intrinsic matrix, $\{\mathbf{k}_0, \mathbf{k}_1, \mathbf{k}_2, \mathbf{k}_3, \mathbf{k}_4\}-$ distortion coefficients (optional) $\mathbf{R}-$ rotation matrix and $\mathbf{t}-$ translation vector.

1: For each correspondence $(\mathrm{L}_j, \mathrm{l}_j)$ compute the matrix H_j from (17).
2: Stacking the N sub-matrices 2×12 into a single $2N \times 12$ matrix H.
3: Obtain parameter vector $\mathbf{m}$ by solving the linear system from (17).
4: The projection matrix $\mathbf{M}$ is determined from (16).
5: The camera intrinsic matrix $\mathbf{K}$, rotation matrix $\mathbf{R}$ and translation vector $\mathbf{t}$ are obtained from (10) with QR-decomposition.
6: Reproject the 3D lines $\{\mathbf{L}_j\}$ into the image to obtain the new image lines $\{\mathbf{l}_j\}$.
7: Using the reprojection 2D lines $\{\mathbf{l}_j\}$ and its corresponding distorted points $\{\mathbf{x}_d^{ji}\}$ form a linear system equations as in Equ. (18).
8: Obtain the distortion coefficients $\{\mathbf{k}_0, \mathbf{k}_1, \mathbf{k}_2, \mathbf{k}_3, \mathbf{k}_4\}$ by solving the linear system equations obtained in the previous step.
9: Assemble the distortion coefficients with the close-form solution and using the Levenberg–Marquardt algorithm to jointly refine the projection matrix $\mathbf{M}$ and distortion coefficients by minimizing the Equ. (19).

Table 1 Camera intrinsic parameters and lens distortion coefficients setting

f_x	f_y	c_x	c_y	k_0	k_1	k_2	k_3	k_4
800	800	320	240	0.5	-0.4	0.4	0	0

Experimental Results

In this section, to validate the proposed method for camera calibration with radial and tangential distortion we conduct the synthetic and real-world experiments. In the synthetic experiments, we calibrate the camera with distortion under different noise levels and compare the corrected images provided by the proposed method and the ground truth. The results show the DLT-lines is robust to noise and not only straightens the lines but also corrects the corresponding points that lie on the lines to the corrected position. On the other hand, the proposed method is tested on the real data by deploying it to calibrate the stereo cameras as it is a full camera calibration method, which estimates intrinsic, extrinsic(*e.g.*, rotation and translation) and distortion parameters simultaneously.

Synthetic Data Experiments

The experiments are carried out under various levels of image noise. The resolution of the synthetic image is 640×480 pixels and the setup of the simulate camera parameters with distortion are depicted in Table 1. The principal point of the camera is located at the image center $(c_x, c_y) = (320, 240)$. The effective focal lengths are $(f_x, f_y) = (800, 800)$ pixels. In terms of the tangential coefficients, we set the last two of them to be zeros as only the first two are considered in practices. The non-coplanar lines are selected in the 3D box that is placed in front of the camera, as shown in Fig. 2. The original point of the reference coordinate system is set in the center of the 3D box. The translation vector is set to be $\mathbf{T} = [0 \quad 0 \quad 40]^T \, dm$. The rotation matrix is set to be an identity matrix $\mathbf{R} = \mathbf{I}_{3\times3}$.

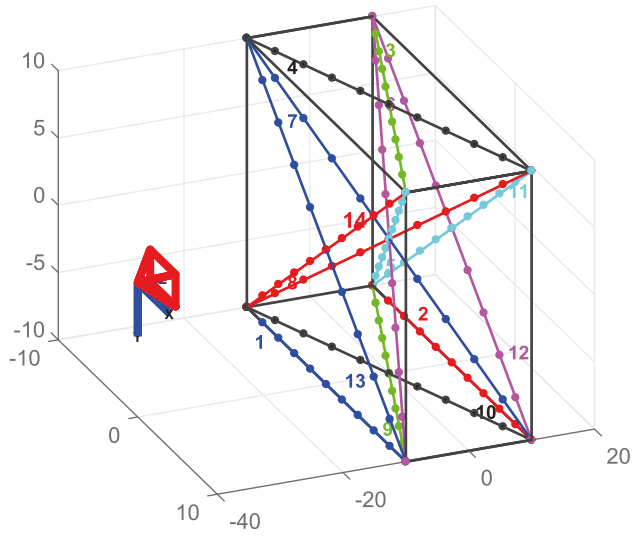

Fig. 2 Setup of the simulate experiments. The 3D box is placed in front of the camera. The 14 selected lines are denoted with various colors and the corresponding number

White Gaussian noise with a standard deviation ranging from 0 to 2.0 pixels with 0.1 pixels as a step is added to the image points. As shown in Fig. 3(a), the relative error of the principal point and the effective focal length is almost linearly with an increase of image noise. Similar to the intrinsic parameters, the radial and the tangential distortion coefficients error are also increasing almost linearly with the image noise, see Fig. 3(b). The reprojection error is defined as the standard error of reprojection points, it is calculated as follow,

$$E_{rpj} = \sqrt{\frac{1}{P}\sum_{i}^{P} \left\| \pi(\mathbf{M}, \mathbf{X}^i, \mathbf{k}) - x^i \right\|} \tag{20}$$

where x^i denotes the measurement point and $\pi(\bullet)$ denotes reprojection point using the estimated camera parameters.

The reprojection error is reported in Fig. 3(c). The calibration is accomplished with the reprojection error within 1.2 pixels under the noise level of 2.0 pixels. Note that, the reprojection error is more effective to show the accuracy of our method as it computes the extrinsic, intrinsic, and lens distortion model jointly.

To test the proposed method on the aspect of correcting the distorted image lines and points, we conduct the experiments by imaging a plane that consists of 16(8 vertical and 8 horizontal) lines with the aforementioned setup. The distorted images and their corresponding corrected images under the noise level of 0.5 pixels are shown in the Fig. 4. The first row displays the images of lines and their corresponding images of points(20 sampled points) are shown in the second row. The distorted images are reported in the first column and the last two columns are their corresponding corrected images utilizing the ground truth parameters and calibration parameters given by the proposed method, respectively. The ideal image points and lines are marked with green color and their corresponding distortion free points and lines are marked with blue and dark color, respectively. It can be seen that our method not only straightens the curves into straightness lines but also corrects their distorted points to the corrected position as our method obtains the actual distortion coefficients. Besides, as depicted in Fig. 5,

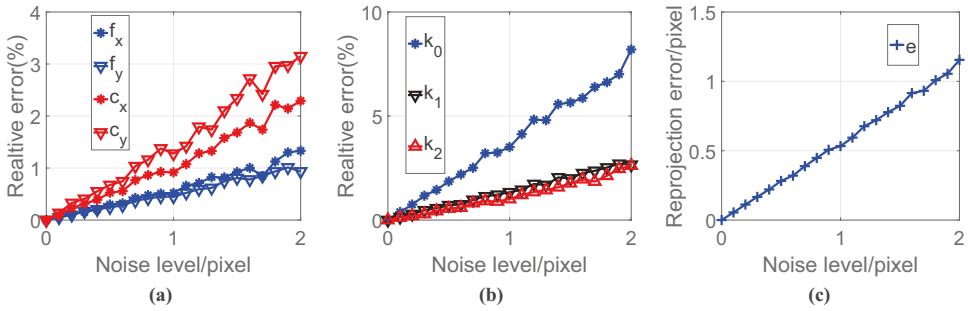

Fig. 3 The reprojection error and the relative error of calibration results against the noise level. **(a)** and **(b)** depict the relative error of the camera intrinsic parameters and lens distortion coefficients, respectively, with increasing noise in image points. **(c)** is the reprojection error of the calibration against increasing image noise

in terms of mean distance error between the corrected points and the ideal points, our method achieves the competitive results with the one utilizing the ground truth parameters to correct the points.

Real Scene Data Experiments

In the real scene data experiments, we compare our method with Zhang's calibration method by calibrating the stereo cameras as the later is widely used in practice. Besides, both are full camera calibration method, which could estimate the extrinsic and intrinsic parameters jointly.

The real images data are acquired with two GoPro cameras(HERO4 Black), which are fixed together. Two cameras are the same and only the medium FOV mode of GoPro cameras is utilized. The vertical and horizontal fields of view(FOVs) are 65.3° and 80.5°, respectively. The image solution is 2560×1920 pixels; the nominal focal length is 3 *mm*; the length of the baseline of two cameras are approximate 150 *mm*. The experimental setup is shown in Fig. 6.

In the experiment, we use the 3D pattern (consists of two 2D chessboard patterns) to construct the required non-coplanar 3D lines for our method. The selected twenty lines are displayed in the Fig. 6(c). We deploy Zhang's method with one similar 2D pattern to calibrate the stereo cameras. To accomplish the stereo calibration, one stereo image pair and sixteen stereo image pairs are captured by the stereo cameras for our method and Zhang's method, respectively.

To compare our method with Zhang's method, we use the same distortion model [28] as Zhang's method, as follow:

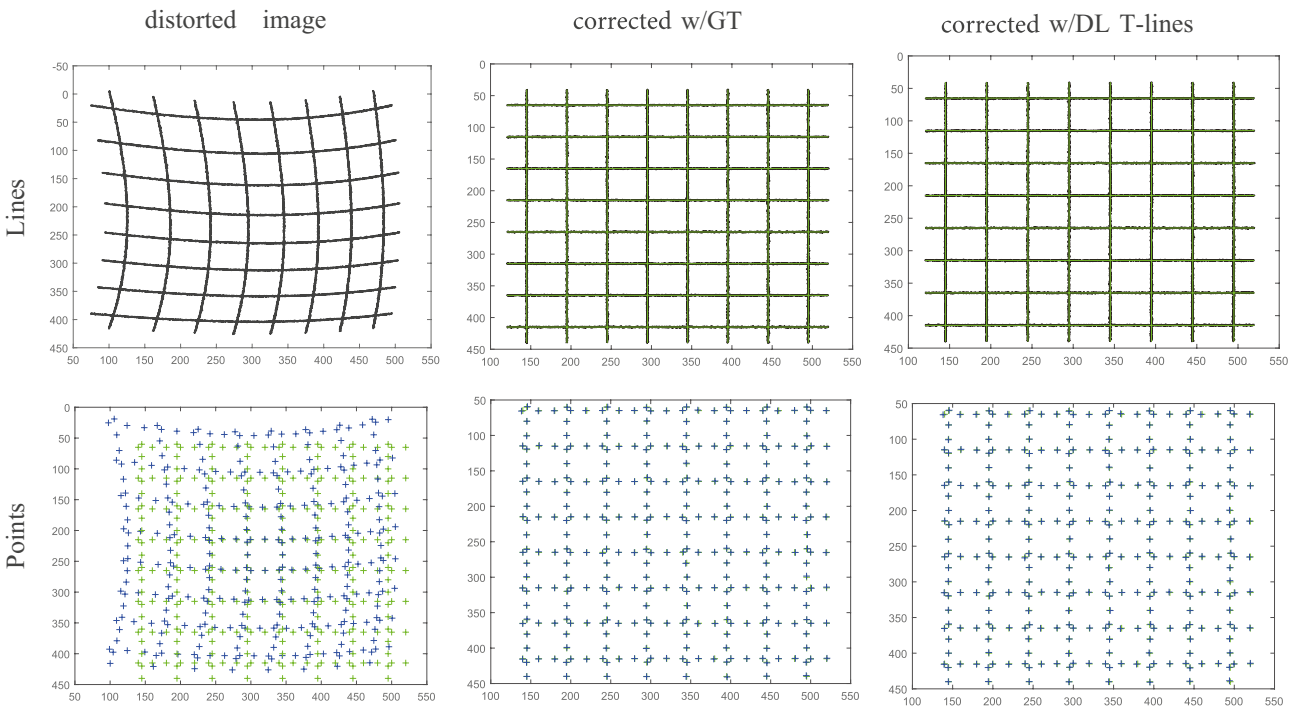

Fig. 4 Corrected image with a noise level of 0.5 pixels. First column: the distorted images of the lines and their corresponding points. Second column: the corrected images utilizing the ground truth parameters. Third column: the corrected images that utilizing the parameters provided by the proposed method. The lines(points) with green color denote the ideal lines(points) and their corresponding lines (points) that corrected with given parameters are marked with dark(blue) color

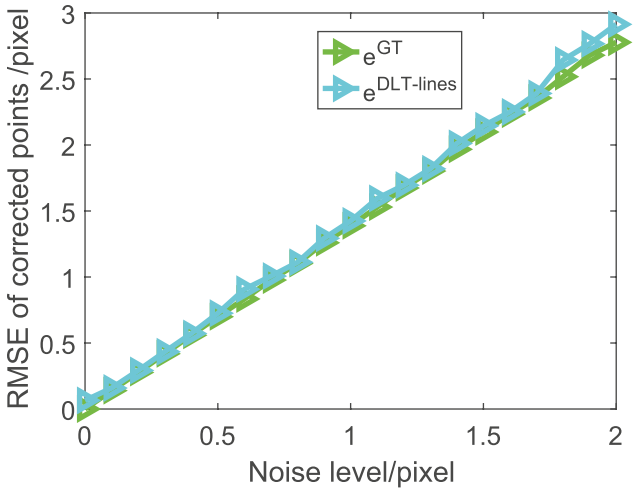

Fig. 5 The root mean sqrt error between the ideal image points and the corresponding corrected points corrected by given parameters. The green color and cyan color denote the correction error given by the ground truth parameters and the parameters provided by the proposed method

$$\begin{cases} \delta_x = f_x[(k_0 r^2 + k_1 r^4 + k_4 r^6)u + 2k_2 uv + k_3(2u^2 + r^2)] \\ \delta_y = f_y[(k_0 r^2 + k_1 r^4 + k_4 r^6)v + 2k_3 uv + k_2(2v^2 + r^2)] \end{cases} \tag{21}$$

where the u, v and r are the same as equation (3); k_0, k_1 and k_4 are the coefficients of radial distortion; k_2 and k_3 are the coefficients of tangential distortion. The k_4 is set to be zero and is not to be calculated for both methods in the experiments, since it is related to the high order of radial distortion and is usually to be ignored in practice.

Table 2 shows the calibration results given by our method and Zhang's method. The unit of effective focal lengths (f_x,f_y) and principal points (c_x, c_y) are pixels. k_0, k_1 and k_4 are the radial distortion parameters, while the k_2 and k_3 are the tangential distortion parameters. **R** and **t** are, respectively, the rotation and translation from the left camera to the right camera. The rotation is denoted by the Rodrigues parameters. The unit of translation coordinate is millimeter.

Figure 7 shows the corrected image points and lines given by our method. The lines and the points marked with green color are the corrected ones computed by the intrinsic and distortion parameters shown in Table 2. The ones marked with dark and blue color are their corresponding distorted lines and points. After the calibration and correction, the lines are straightened and their corresponding points are corrected.

In order to validate the accuracy of our calibration results, we prune the image points lying on the selected lines and utilize the rest corrected image points to reconstruct the 3D pattern. Base on the calibration results of stereo cameras in Table 2, we compute the reconstruction 3D pattern points for our method and Zhang's method, respectively. Then, we assess the RMS of reconstruction error as follow:

$$\epsilon_i = \|\mathbf{T}^s \mathbf{X}_i^s - \mathbf{X}_i^{gt}\| \tag{22}$$

where $\mathbf{X}_i^s$ and $\mathbf{X}_i^{gt}$ are, respectively, the reconstruction points and its corresponding ground truth. The rigid transformation $\mathbf{T}^s$ denotes the transformation from the stereo cameras to the 3D pattern, it is obtained by minimizing the distance error $\|\mathbf{T}\mathbf{X}_i^s - \mathbf{X}_i^{gt}\|$.

Figure 8 shows the reconstruction results of our method. The reconstruction results(black circle) are consistent with the ground truth(green points). The RMS of reconstruction error and its median error value are shown in Table 3. The RMS of reconstruction error is 1.00 *mm* using our method, and the RMS of reconstruction error is 0.75 *mm* using Zhang's method. Zhang's method is superior to our method in terms of RMS error as it requires more image pairs (16 image pairs are used in this experiment) to accomplish the calibration of stereo cameras, while only one image pair is needed for our method. The redundant images of the pattern would be easier to cover the fields of view, which is helpful for handling the extreme

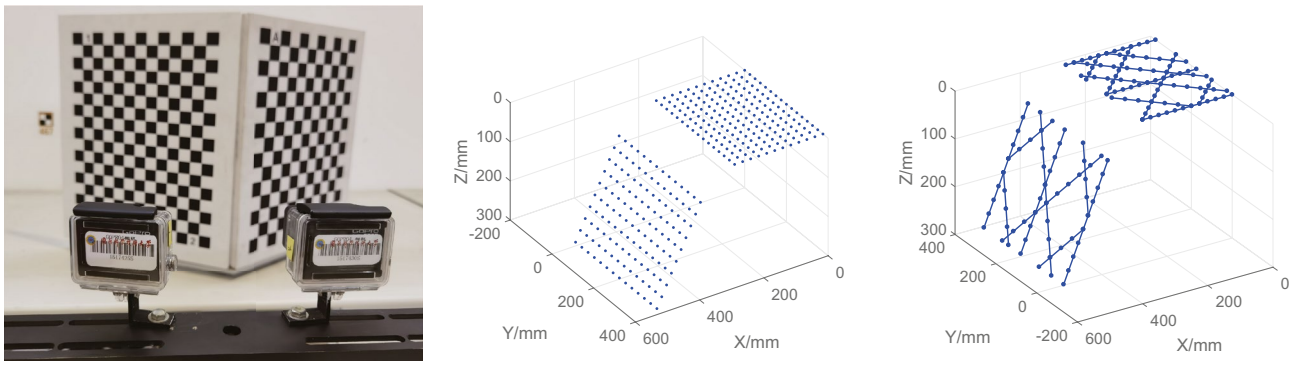

(a) **(b)** **(c)**

Fig. 6 The experimental setup of stereo cameras calibration. **(a)** is the 3D pattern in front of the stereo cameras. **(b)** displays the 3D points of the calibrated pattern. **(c)** shows the selected non-coplanar lines for our calibration method

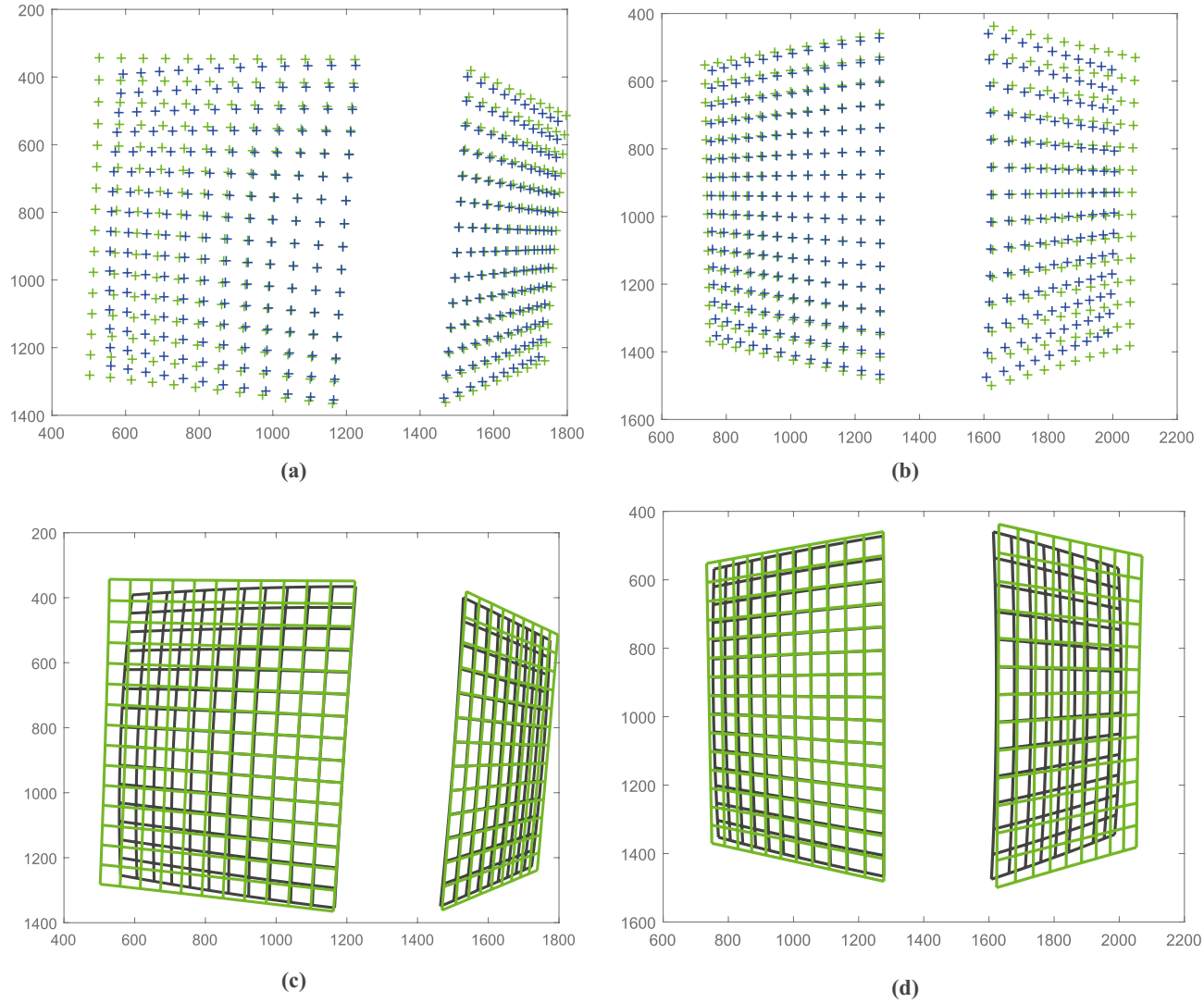

Fig. 7 The image pairs of corrected points and lines. The first and second columns are the images of the left camera and the right camera, respectively. The blue points are the distorted points captured by the cameras and their corresponding corrected points are marked with green color. The black lines displayed in the second row are the distorted lines and the green lines are their corresponding corrected lines

distorted points that lie on the image margin. In terms of median reconstruction error, the error of our method is 0.26 *mm* and the error of Zhang's method is 0.34 *mm*. Our method is superior to Zhang's method on the aspect of median error. In short, our method is feasible and is on par with the widely used method while requires only a single image or one image pair.

Table 2 The stereo calibration results of our method and Zhang's method. The number in the table is three decimal places. The k_4 is set to be zero and is not to be calculated for both method

	Parameters	Our method	Zhang's method
Left camera	(f_x, f_y)	(1494.602, 1482.520)	(1512.406, 1499.820)
	(c_x, c_y)	(1275.488, 905.560)	(1271.275, 914.956)
	(k_0, k_1, k_4)	(−0.262, 0.096, 0.000)	(−0.273, 0.107, 0.000)
	(k_2, k_3)	(0.001, 0.002)	(0.000, 0.001)
Right camera	(f_x, f_y)	(1494.927, 1482.557)	(1516.055, 1503.669)
	(c_x, c_y)	(1239.726, 952.536)	(1229.600, 975.385)
	(k_0, k_1, k_4)	(−0.265, 0.111, 0.000)	(−0.275, 0.115, 0.000)
	(k_2, k_3)	(−0.003, −0.001)	(0.000, 0.000)
Rigid transformation	R	(−0.048, 0.349, −0.047)	(−0.031, 0.349, −0.043)
	t	(−143.650, 0.561, 20.225)	(−143.341, 4.399, 22.251)

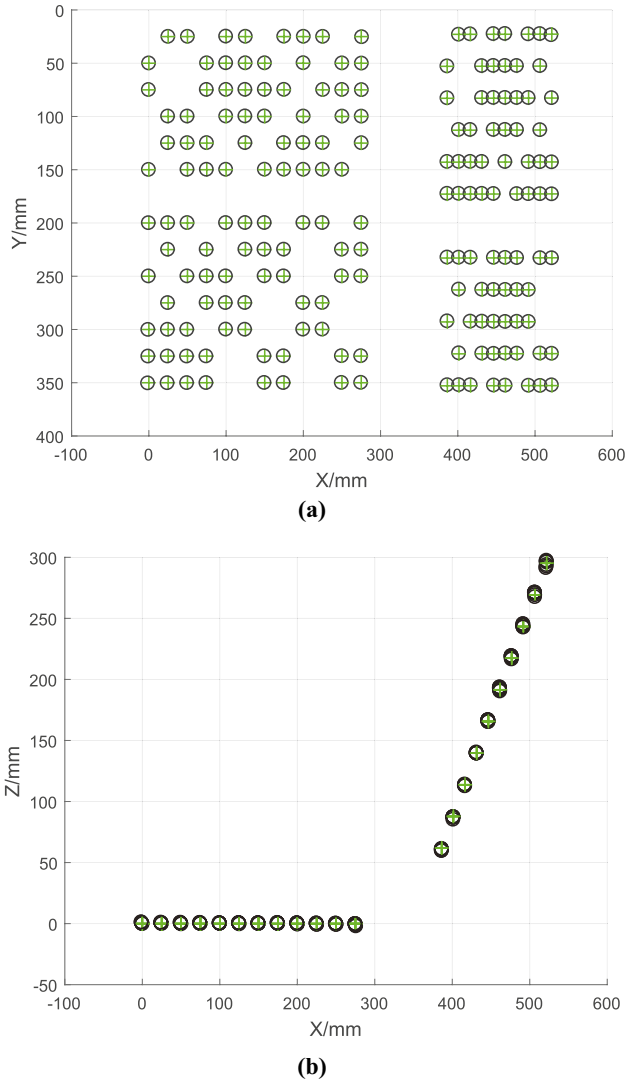

Fig. 8 3D reconstruction results of our method. **(a)** and **(b)** are the front view and vertical view of 3D reconstruction results. The black circle points are the reconstruction results and the green points are their corresponding ground truth

Table 3 The reconstruction error of our method and Zhang's method

Methods	RMSE (*mm*)	Median error (*mm*)
Zhang's method	0.75	0.34
Our method	1.00	0.26

Summarily, the synthetic data experiment shows that our method is not only straightening the distorted lines to be straightness but also correcting their corresponding points as our method computes the distortion parameters by utilizing the reprojection lines. The real scene data experiments validate that our method is practical for work site use. Besides, comparing with the widely used method, it can provide competitive calibration results. On the other hand, since only a single image is required for camera calibration, it requires the 3D pattern is placed to cover the whole fields of view.

Conclusions

In this paper, we propose a full camera calibration method for the optical measurement in experimental mechanics. We focus on camera calibration with lens radial and tangential distortion using the 3D lines. We utilize a set of non-coplanar 3D lines and their corresponding 2D image lines for estimating the camera extrinsic and intrinsic parameters simultaneously. The solutions of lens radial and tangential distortion parameters are derived linearly and analytically by utilizing the 2D reprojection lines. A non-linear parameter optimization algorithm is applied to jointly refine all the parameters for improving the calibration results.

The synthetic data experiment and real scene data experiment validate that the proposed method could provide competitive calibration results. The proposed method is practical for work site as it is easy to be implemented. The non-coplanar lines used in the method can be made by using the 3D pattern. A real scene can also be utilized directly for the case of large scale scenes, such as the straight edges of windows, doors and buildings.

A limitation of the proposed method is that it cannot handle the extreme cases, such as the lens with severe distortion and line is mapped into a point, which results in not enough image lines are detected. The proposed method needs a single image with six or more non-coplanar and control lines. Future work includes involving the degeneration detection scheme and combining the lines and points to increase the accuracy of the calibration.

Acknowledgements This work was supported in part by the National Natural Science Foundation of China, under Grant No. 11872070 and Grant No. 11902349.

Declarations

Conflicts of interests The authors declare that they have no conflict of interest.

References

1. Sutton MA, Orteu JJ, Schreier H (2009) Image correlation for shape, motion and deformation measurements: basic concepts, theory and applications. Springer Science & Business Media

2. Yasmeen F, Balcaen R, Sutton MA, Debruyne D, Rajan S, Schreier HW (2018) Sensitivity of in-plane strain measurement to calibration parameter for out-of-plane specimen rotations. Exp Mech 58(7):1115–1132
3. Siddiqui M, Ahmed M (2014) An out-of-plane motion compensation strategy for improving material parameter estimation accuracy with 2d field measurements. Exp Mech 54(7):1259–1268
4. Zhao X, Sutton MA, Zhang H, Deng X, Reynolds AP, Ke X, Schreier H (2015) Stereo image based motion measurements in fluids: experimental validation and application in friction extrusion. Exp Mech 55(1):177–200
5. Balcaen R, Reu P, Lava P, Debruyne D (2018) Influence of camera rotation on stereo-dic and compensation methods. Exp Mech 58(7):1101–1114
6. Luo P, Chao Y, Sutton M, Peters WH (1993) Accurate measurement of three-dimensional deformations in deformable and rigid bodies using computer vision. Expe Mech 33(2):123–132
7. Reu P (2013) A study of the influence of calibration uncertainty on the global uncertainty for digital image correlation using a monte carlo approach. Expe Mech 53(9):1661–1680
8. Silva M, Ferreira R, Gaspar J (2012) Camera calibration using a color-depth camera: Points and lines based dlt including radial distortion. In Proc. of IROS Workshop in Color-Depth Camera Fusion in Robotics
9. Tsai R (1987) A versatile camera calibration technique for high-accuracy 3d machine vision metrology using off-the-shelf tv cameras and lenses. IEEE J Rob Auto 3(4):323–344
10. Zhang Z (2000) A flexible new technique for camera calibration. IEEE Trans Patt Anal Mach Intell 22(11):1330–1334
11. Guan B, Yu Y, Su A, Shang Y, Yu Q (2019) Self-calibration approach to stereo cameras with radial distortion based on epipolar constraint. Appl Opt 58(31):8511–8521
12. Hemayed EE (2003) A survey of camera self-calibration. In Proceedings of the IEEE Conference on Advanced Video and Signal Based Surveillance, 2003, IEEE pages 351–357
13. Liu D, Liu X, Wang M (2016) Camera self-calibration with lens distortion from a single image. Photogram Eng Rem Sens 82(5):325–334
14. Liu W, Wu S, Wu X, Zhao H (2019) Calibration method based on the image of the absolute quadratic curve. IEEE Access 7:29856–29868
15. Zhou F, Cui Y, Gao H, Wang Y (2013) Line-based camera calibration with lens distortion correction from a single image. Opt Lasers Eng 51(12):1332–1343
16. Ahmed M, Farag A (2005) Nonmetric calibration of camera lens distortion: differential methods and robust estimation. IEEE Trans Imag Proc 14(8):1215–1230
17. Benligiray B, Topal C (2016) Blind rectification of radial distortion by line straightness. In 2016 24th European Signal Processing Conference (EUSIPCO), IEEE pages 938–942
18. Brauer-Burchardt C, Voss K (2001) A new algorithm to correct fish-eye-and strong wide-angle-lens-distortion from single images. In Proceedings 2001 International Conference on Image Processing (Cat. No. 01CH37205), IEEE 1:225–228
19. Devernay F, Faugeras O (2001) Straight lines have to be straight. Mach Vis Appl 13(1):14–24
20. Zhang Z, Zhao R, Liu E, Yan K, Ma Y (2018) A single-image linear calibration method for camera. Measurement 130:298–305
21. Galego R, Ortega A, Ferreira R, Bernardino A, Andrade-Cetto J, Gaspar J (2015) Uncertainty analysis of the dlt-lines calibration algorithm for cameras with radial distortion. Comp Vis Imag Und 140:115–126
22. El-Melegy MT, Farag AA (2003) Nonmetric lens distortion calibration: Closed-form solutions, robust estimation and model selection. In null, page 554. IEEE
23. Adbel-Aziz Y (1971) Direct linear transformation from comparator coordinates into object space coordinates in close-range photogrammetry. Proceedings of the Symposium on Close-Range Photogrammetry (Am Soc Photogram) 1971:1–18
24. Lecrosnier L, Boutteau R, Vasseur P, Savatier X, Fraundorfer F (2019) Camera pose estimation based on pnl with a known vertical direction. IEEE Rob Auto Lett 4(4):3852–3859
25. Xu C, Zhang L, Cheng L, Koch R (2016) Pose estimation from line correspondences: A complete analysis and a series of solutions. IEEE Trans Patt Anal Mach Intell 39(6):1209–1222
26. Weng J, Cohen P, Herniou M et al (1992) Camera calibration with distortion models and accuracy evaluation. IEEE Trans Patt Anal Mach Intell 14(10):965–980
27. Henderson HV, Searle SR (1981) The vec-permutation matrix, the vec operator and kronecker products: A review. Lin Multilin Algeb 9(4):271–288
28. Duane CB (1971) Close-range camera calibration. Photogramm Eng 37(8):855–866